Figures and figure supplements

Homeostatic plasticity fails at the intersection of autism-gene mutations and a novel class of common genetic modifiers

Özgür Genç *et al*

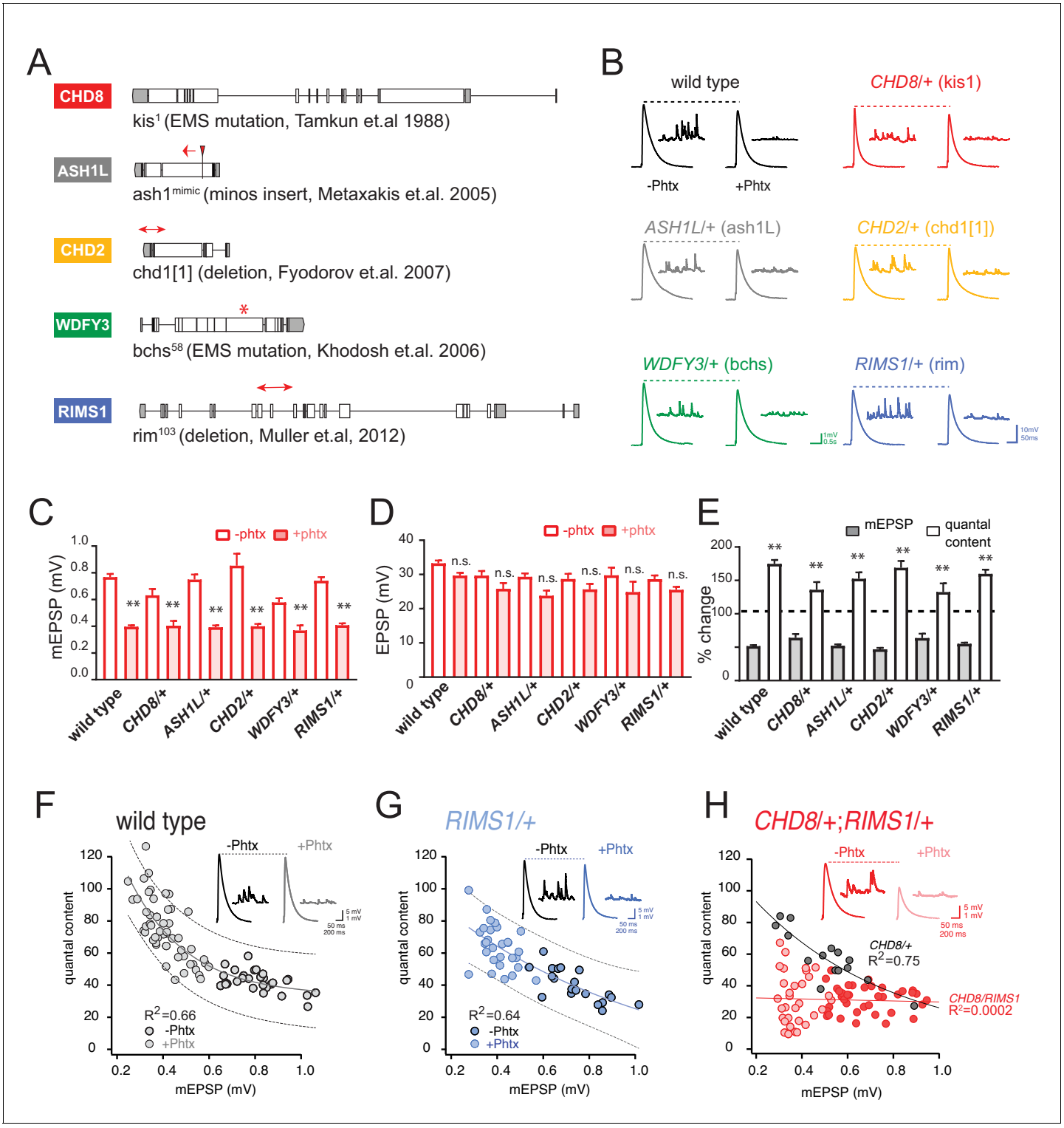

Figure 1. Heterozygous ASD gene mutations do not affect baseline transmission or PHP. (**A**) Schematic of the *Drosophila* locus for *CHD8, ASH1L, CHD2, WDFY3* and *RIMS1* with gene disruptions indicated. (**B**) Representative EPSP and mEPSP traces for indicated genotypes (+ / - PhTx for each genotype, left traces and right traces respectively) (**C–D**) Quantification of mEPSP amplitude (**C**) and EPSP amplitude (**D**) in the absence and presence of PhTx (open and filled bars respectively). (**E**) The percent change of mEPSP and quantal content as indicated, comparing the presence and absence of PhTx for each genotype with Student's t-test (two tail), *p<0.05, **p<0.01. Sample sizes for data reported (**C–E**) are as follows (n reported for each genotype -/+ PhTx): *wild type*: n = 36/47; *CHD8/+*: n = 7/8; *ASH1L/+*: n = 15/25; *WDFY3/+*: n = 8/7; *CHD2/+*: n = 8/19; *RIMS1/+*: n = 20/30. (**F–H**) Scatter plots of quantal content (*y* axis) versus mEPSP amplitude (*x* axis) for wild type (left), *RIMS1/+* mutant (middle) and the *CHD8/+; RIMS1/+* double

Figure 1 continued on next page

Figure 1 continued

heterozygous mutant. Each symbol represents an individual muscle recording. Inset: representative traces (+ / - PhTx). Exponential data fit (black line, R^2-value inset, calculated based on a linear fit). Dashed lines encompass 95% of all data (absent in (**H**) for clarity). Below each graph (**F–H**), boxes display percent PHP (+ / - PhTx for each genotype), statistical values compared to baseline (**H**).

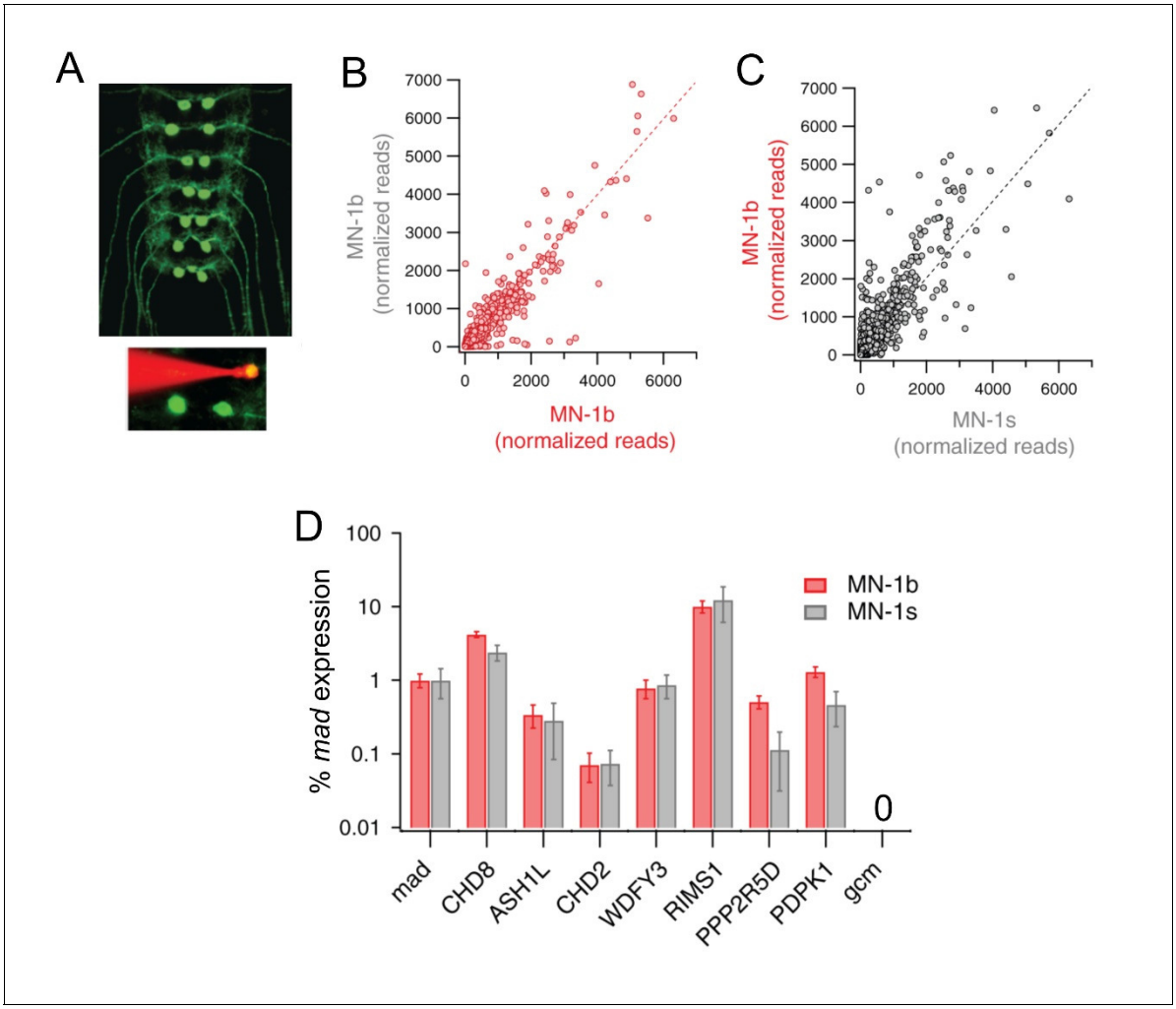

Figure 1—figure supplement 1. Patch-Seq analysis of gene expression in type 1b and type 1 s motoneurons. (**A**) Image of the larval central nervous system with expression of *UAS-CD8-GFP* driven by *MN1-GAL4*. Inset, a rhodamine filled patch electrode targets a single identified motoneuron for excision and sequencing (see Materials and methods). (**B**) Differential gene expression analysis for two different experiments comparing MN1b (three biological replicates each). Most data rely on unity as expected. (**C**) Comparison of gene expression for type 1b and type 1 s motoneurons. (**D**) Expression analysis of ASD gene orthologs in type 1b and type 1 s motoneurons in the third larval instar taken from the patch seq data. Expression is normalized to the well-established, motoneuron-expressed transcription factor *mothers against decapentaplegic* (*mad*). As confirmation of predicted gene expression we note the absence of expression for *glial cells missing* (*gcm*).

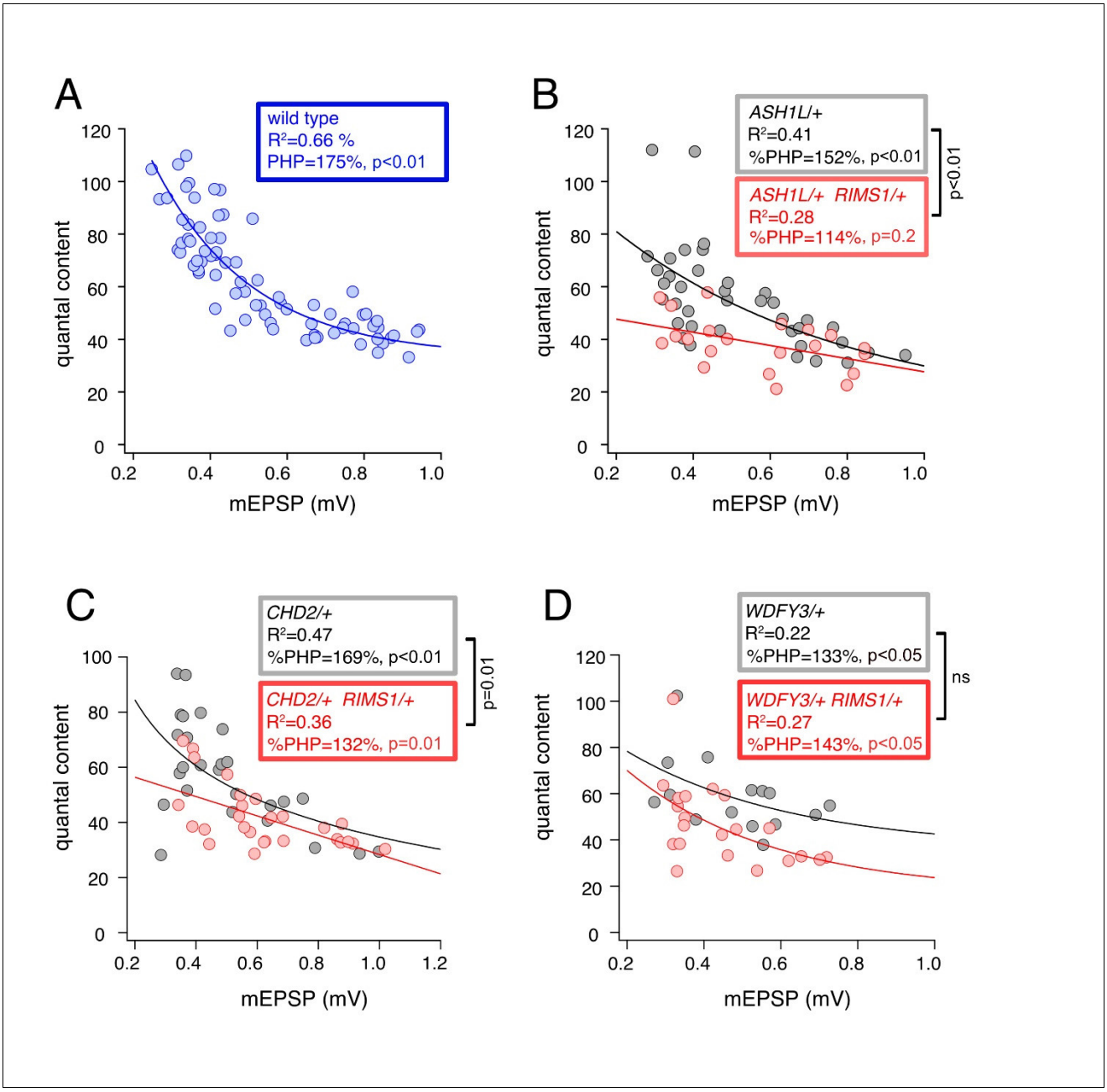

Figure 1—figure supplement 2. Double-heterozygous gene mutation combinations impair homeostatic plasticity. (**A–D**) Scatter plots of quantal content (*y* axis) versus mEPSP amplitude (*x* axis) for **A**) *wild type*; **B**) *ASH1L/+, RIMS1/+* double heterozygous mutant (red) and *ASH1L/+* heterozygous mutant (grey); **C**) *CHD2/+; RIMS1/+* double heterozygous mutant (red) and *CHD2/+* heterozygous mutant (grey); **D**) *WDFY3/+; RIMS1/+* double heterozygous mutant (red) and *WDFY3/+* heterozygous mutant (grey). Each symbol represents an individual muscle recording. Exponential and line data fits (straight line, R^2-value inset). Boxes show statistics for curve fits and percent PHP expression (plus/minus PhTx). P-values within boxes report the statistical significance of PHP over genotypic baseline. P-values outside boxed compare PHP expression between genotypes.

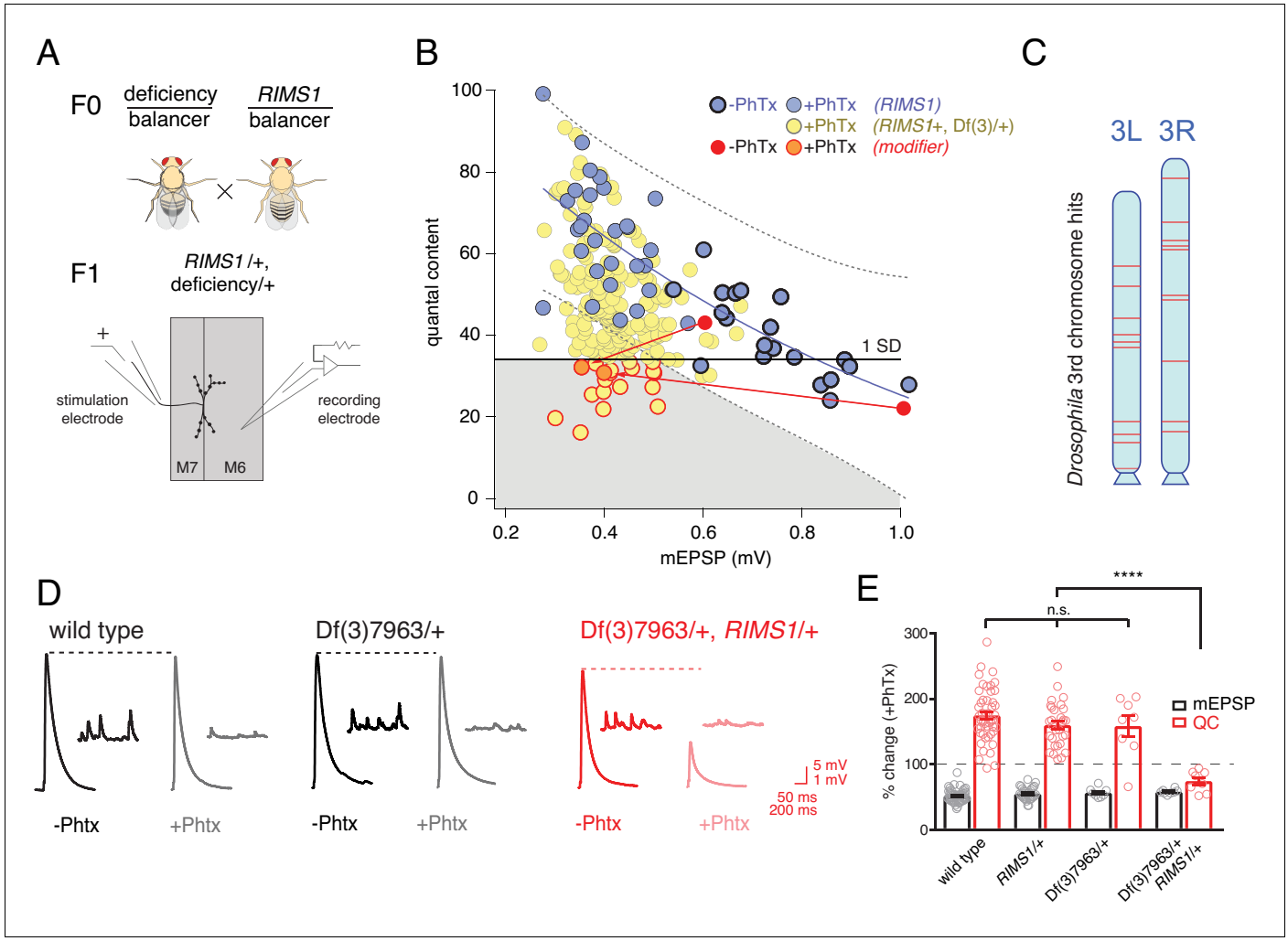

Figure 2. Screen for common genomic modifiers of ASD-associated gene mutations. (**A**) Diagram of genetic screen. (**B**) Screen results are shown with yellow circles representing average data per genotype. Fit (solid blue line) and confidence interval (dotted lines encompassing 95% of all data) from *RIMS1/+* are overlaid. Black horizontal line defines one standard deviation from population mean (yellow circles). Gray area encompasses potential hits residing outside the *RIMS1/+* confidence interval and below the solid line. Two modifiers are shown in the absence (dark red circles) and presence of PhTx (light red circles, dark outline) (**C**) Approximate location of hits (red lines) on chromosome 3. (**D**) Representative traces for indicated genotypes in the presence and absence of PhTx as indicated. (**E**) Average percent change in mEPSP amplitude (gray bars) and quantal content (red bars) in presence of PhTx compared to baseline. One-way ANOVA and posthoc Tukey's multiple comparisons; ****p<0.0001 for quantal content (QC).

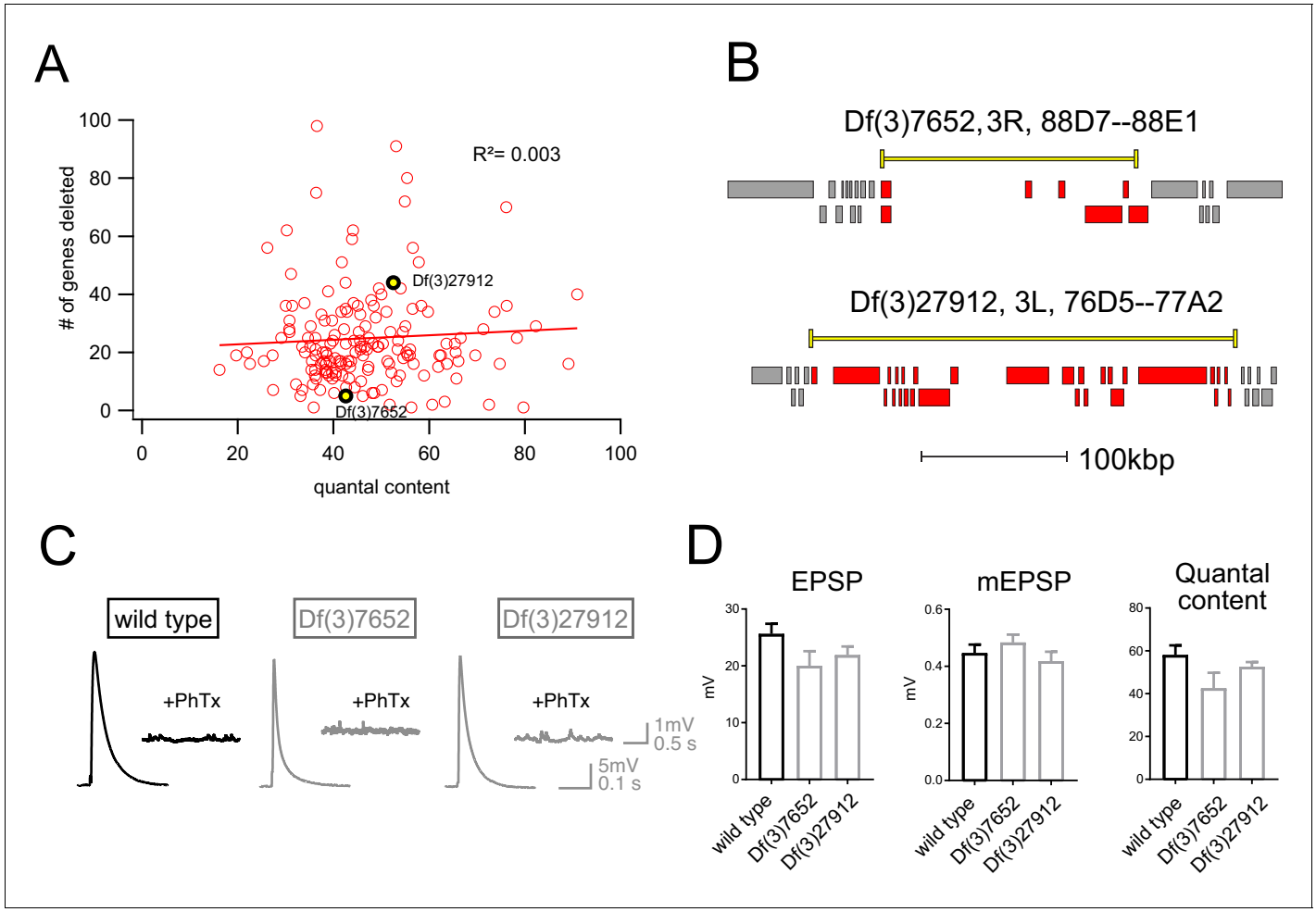

Figure 3. Absence of an additive effect of gene heterozygosity on synaptic transmission or PHP. (**A**) Scatter plot showing the number of genes deleted (*y* axis) versus quantal content (*x* axis) in the presence of PhTx for all deficiencies tested. Each circle represents average data from an individual muscle recording for an individual deficiency. Red line shows the fit with a Pearson coefficient of 0.003. (**B**) Schematic of two deficiency alleles showing the extent of the deletion (yellow bars) and the genes deleted (red boxes) (**C**) Representative EPSP and mEPSP traces for indicated genotypes **D**) Quantification of EPSP, mEPSP amplitude and quantal content for the indicated genotypes. All deficiencies recorded as heterozygous mutations in the presence of *RIMS1*/+).

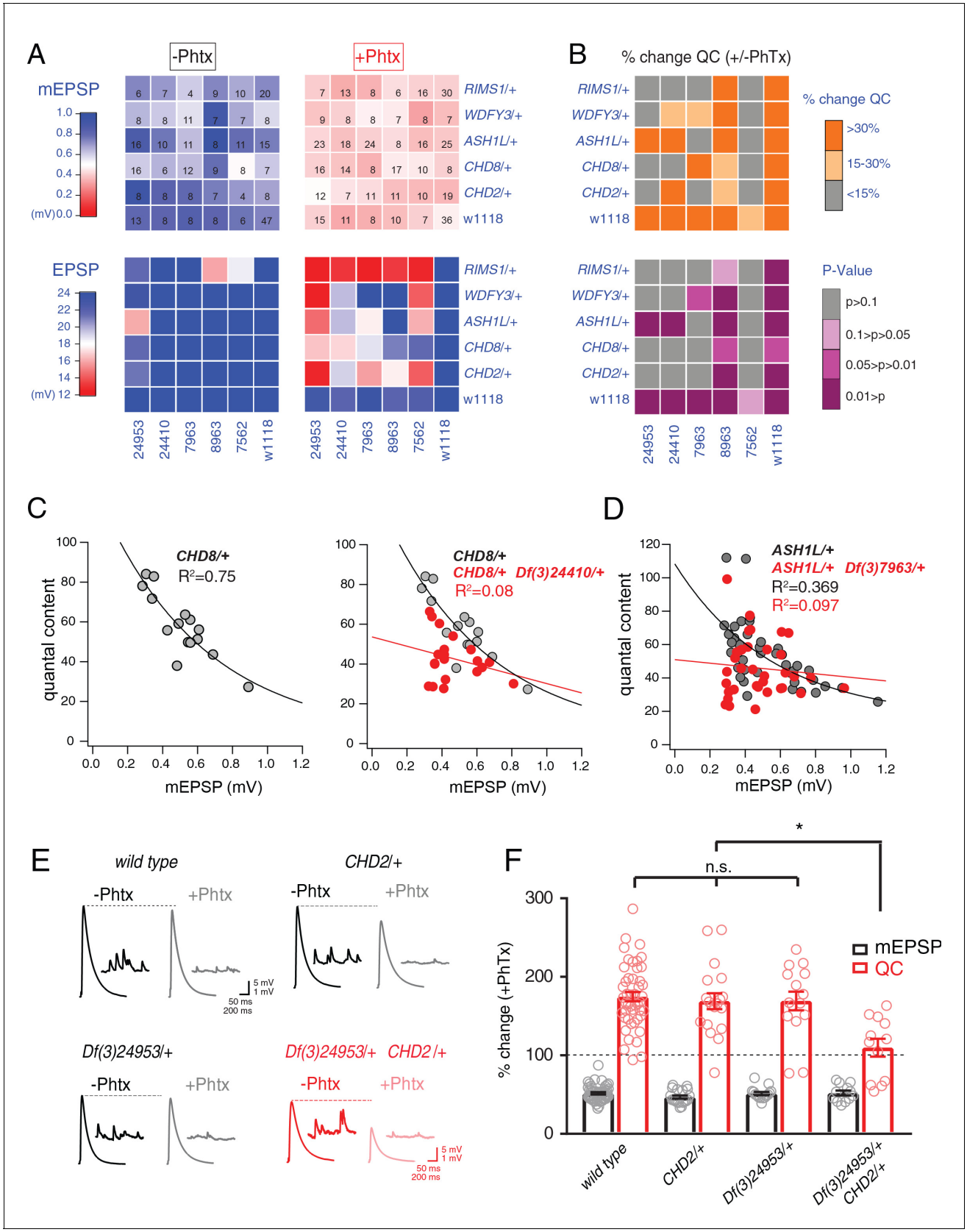

Figure 4. Identification of common modifiers of diverse ASD-associated mutations. (**A**) Genetic interaction matrix showing average mEPSP (top two matrix) and EPSP (bottom two matrix) amplitudes in the absence (left) and presence (right) of PhTx, as indicated. Values are according to lookup codes

Figure 4 continued on next page

Figure 4 continued

at left. Each individual box represents average data for a double-heterozygous mutant at intersection of x and y axes. Sample size (number of NMJ recordings) is displayed for each box (top) and are identical below (bottom). (**B**) Top matrix (orange and gray) is organized as in (A). Average percent change in quantal content (+ PhTx) compared to baseline (- PhTx), values according to lookup code. Bottom panel, shows data from top panel re-plotted diagramming p-values for the observed percent change in quantal content (+ / - PhTx), values according to lookup code. Student's t-test (two tail) comparing each genotype + / - PhTx. (**C**) Scatter plots of quantal content (*y* axis) versus mEPSP amplitude (*x* axis) for *CHD8/+* (left), and *CHD8/+;Df(3)24410/+*. (**D**) Scatter plot as in (C) for *ASH1L/+* and *ASH1L/+,/Df(3)7963/+*. Each dot represents average data from an individual muscle recording. Fits as indicated. R^2 values as indicated (calculated based on linear fit). (**E**) Representative traces for indicated genotypes (+ / - PhTx) (**F**) Percent change in mEPSP (gray bars) and quantal content (red bars) in presence of PhTx compared to baseline. One-way ANOVA and posthoc Tukey's multiple comparisons; *p<0.05.

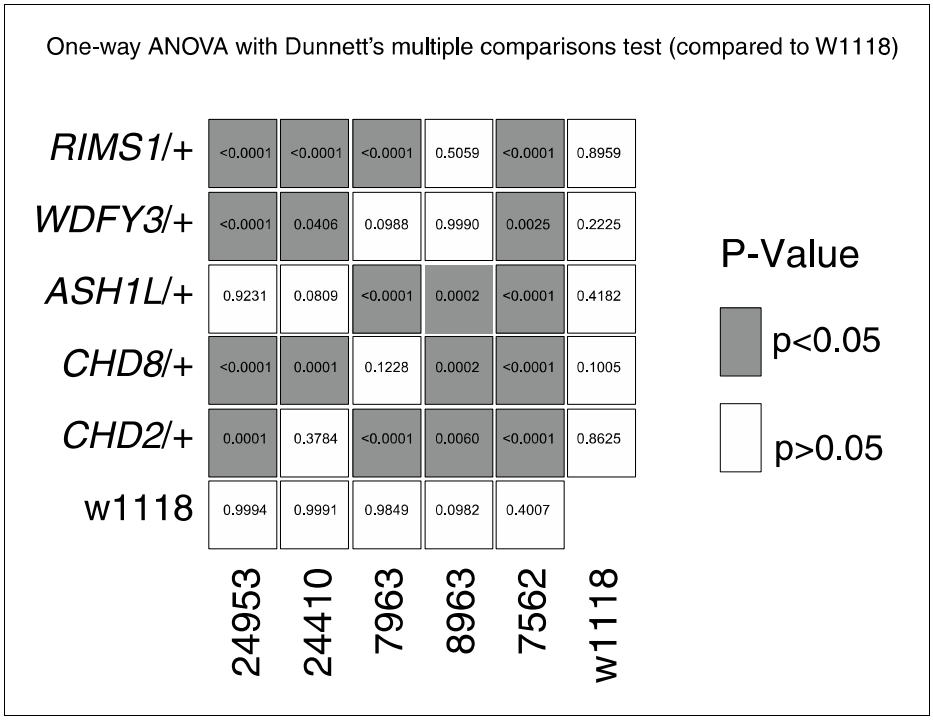

Figure 4—figure supplement 1. One-way ANOVA with Dunnett's multiple comparisons test (compared to *w1118*). Genetic interaction matrix showing color-coded p-values from One-way ANOVA with Dunnett's multiple comparisons test. Each individual box represents p-values for the comparison of percent change in quantal content for a double-heterozygous mutant at intersection of x and y axes against wild type (*w1118*). Values are according to lookup codes at right (gray color indicates genotypes which have statistically significant difference, white color indicates no difference compared to *w1118*). Note that all comparisons indicated in gray are highly statistically significant with $p<0.001$, with the exception of two matrix element: *Df(24410)/+* with *WDFY3/+* is $p=0.0406$ and *Df(7562)/+* with *WDFY3/+* is $p=0.0025$.

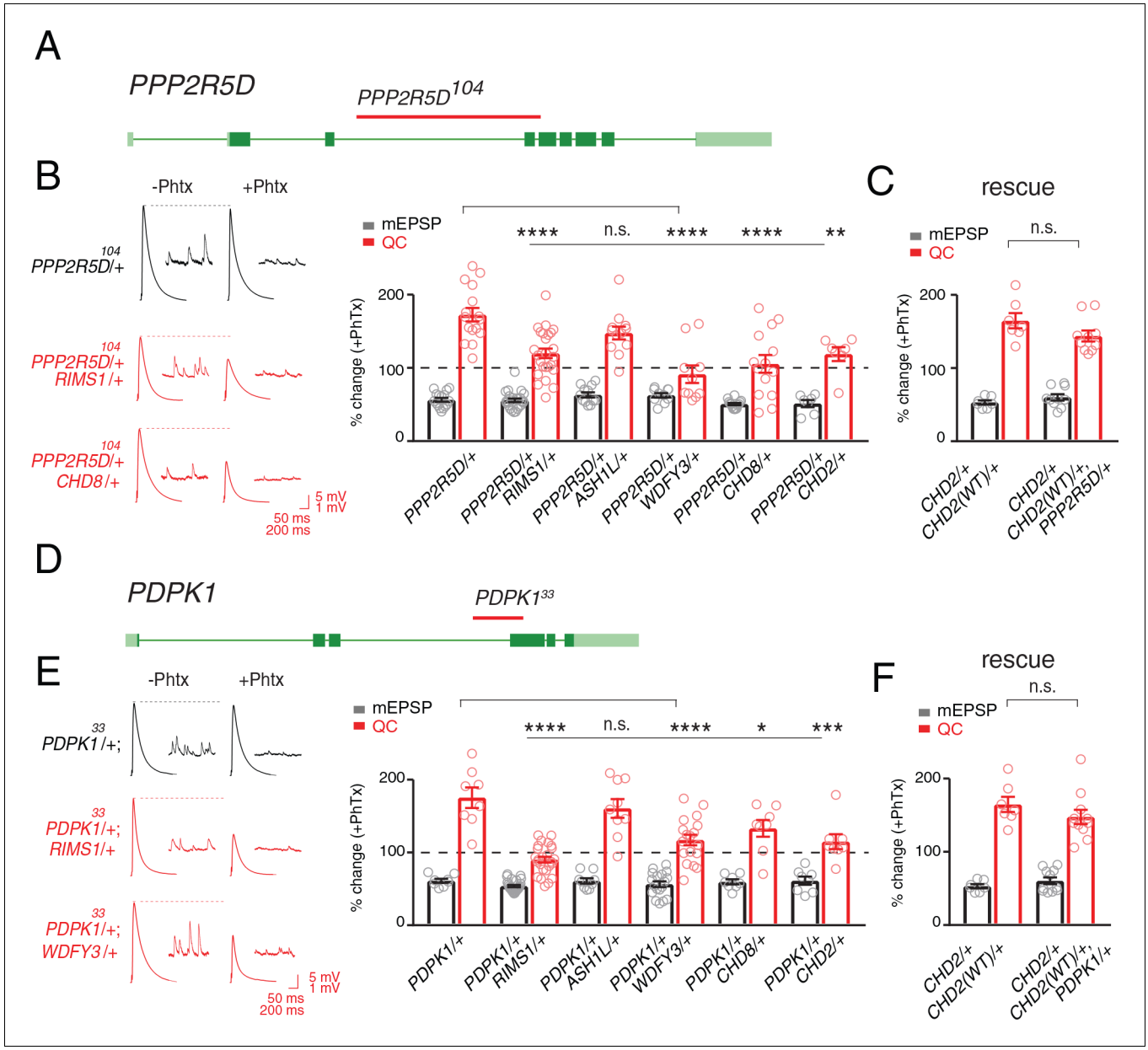

Figure 5. Single genes are common modifiers of diverse ASD-associated mutations. (**A**) Schematic of the *PPP2R5D* gene locus and the *PPP2R5D*^{104} deletion mutation (red horizontal bar). (**B**) Representative traces for indicated genotypes. Bar graph (right) shows percent change in mEPSP (gray) and quantal content (red) (+ / - PhTx). (**C**) Data as in (**B**) for rescue of the double heterozygous *CHD2*/+ and *PPP2R5D*^{104}/+ mutant by incorporation of a *CHD2* translocation (*CHD2*^{WT}/+). (**D**) Schematic of the *PDPK1* gene locus with the *PDPK1*^{33} deletion mutation (red horizontal bar). (**E**) Representative traces for indicated genotypes. Bar graph (right) as in **B**. (**F**) Data as in (**C**) for the genomic rescue of double heterozygous *CHD2*/+ and *PDPK1*^{33}/+ mutants. One-way ANOVA, Dunnett's multiple comparisons *p<0.05, **p<0.01, ***p<0.001, ****p<0.0001 for (**B**) and (**E**), Student's t-test, two-tailed for (**C**) and (**F**), n.s. p>0.05).

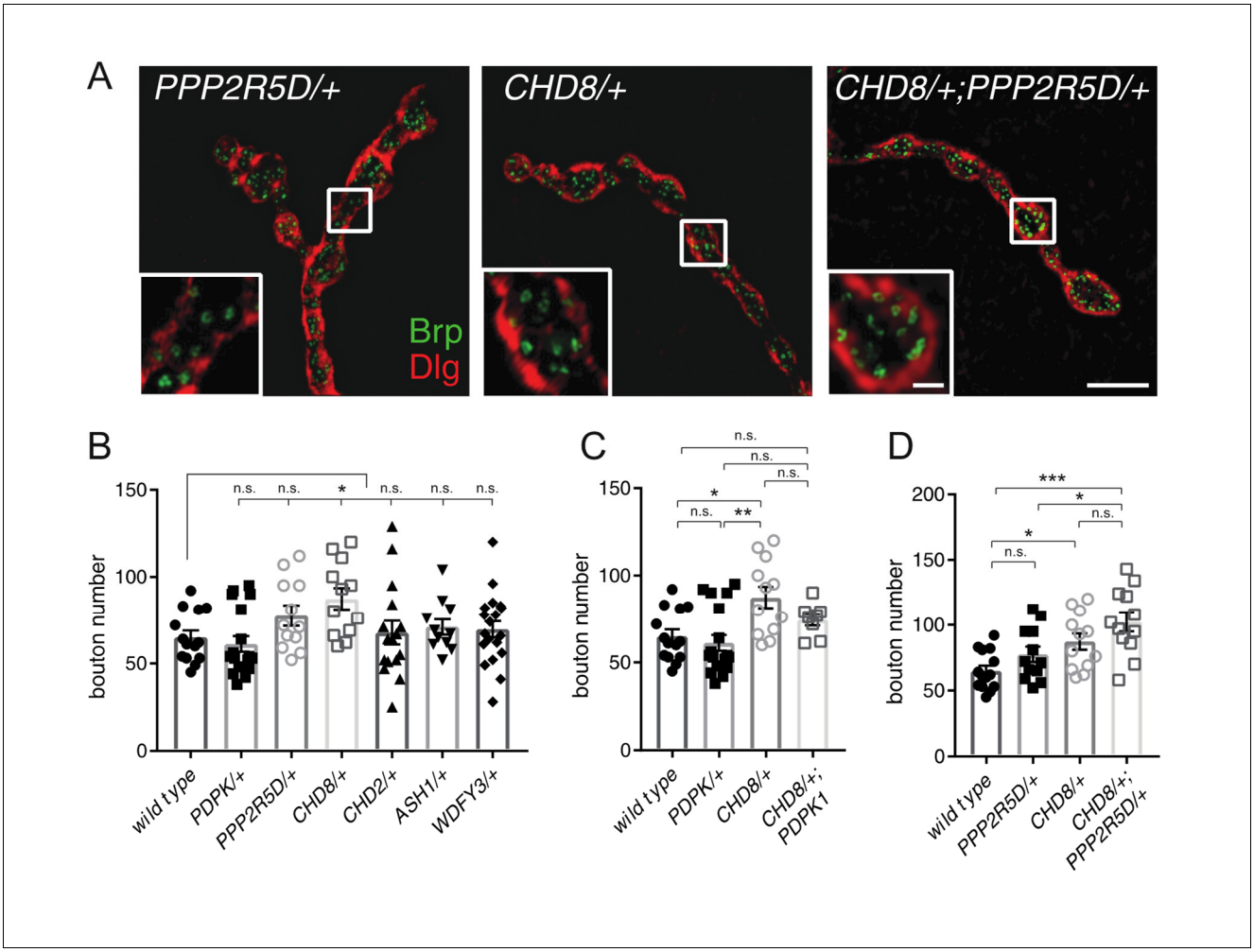

Figure 5—figure supplement 1. Analysis of the NMJ morphology. (**A**) Structured illumination microscopy (SIM) images of neuromuscular junction for indicated genotypes. Insets show single confocal sections. Staining for anti-Brp (green) to mark active zones and anti-Dlg (red) to mark postsynaptic membranes. Scale bars: 5 μm and 1 μm (inset). (**B**) Quantification of bouton number from NMJ (abdominal segments 2 and 3) for the indicated genotypes. One-way ANOVA, Dunnett's multiple comparisons, n.s $p>0.05$; *$p<0.05$ (**C-D**) Data repeated from (**B**) highlighting specific comparisons for genotypes involving the heterozygous *CHD8/+* mutation. One-way ANOVA, Tukey's multiple comparisons, n.s $p>0.05$; *$p<0.05$; **$p<0.01$; ***$p<0.001$. Data acquired and analyzed blind to genotype.

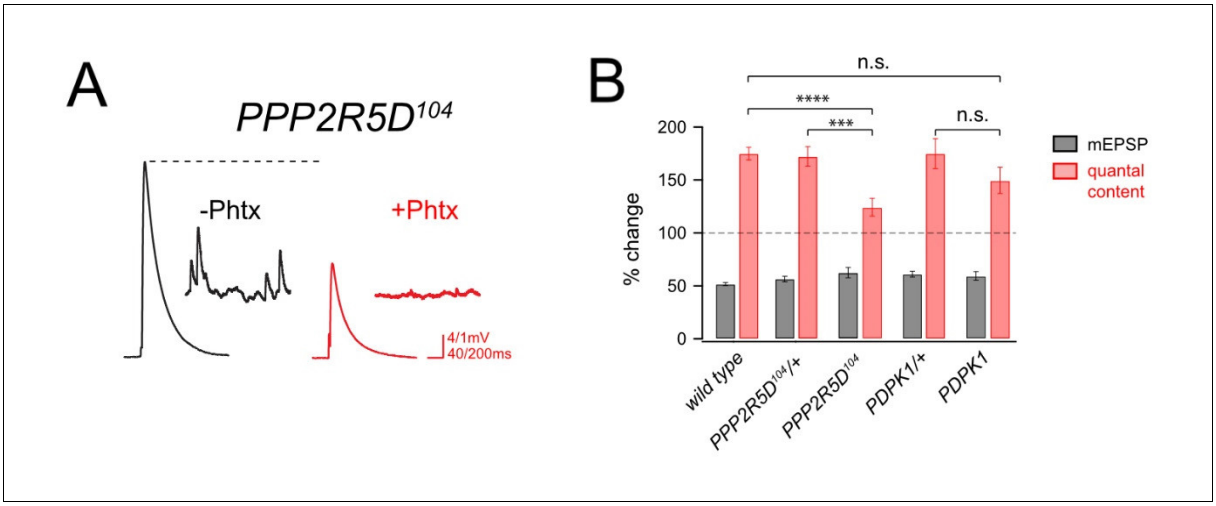

Figure 5—figure supplement 2. A *PPP2R5D* loss-of-function mutation disrupts PHP, but PDPK1 does not. (**A**) Representative mEPSP and EPSP traces for *PPP2R5D*^{104} homozygous mutant (-/+ PhTx) (**B**) Percent change in mEPSP amplitude (gray bars) and quantal content (red bars) with PhTx compared to baseline for the indicated genotypes. Sample size is number of NMJ recorded (two per animal): *wild type* (-PhTx n = 27, +PhTx n = 26), *PPP2R5D*^{104} / + (-PhTx n = 8, +PhTx n = 16), *PPP2R5D*^{104} (-PhTx n = 11, +PhTx n = 15), *PDPK1/+* (-PhTx n = 4, +PhTx n = 8), *PDPK1* (-PhTx n = 9, +PhTx n = 9). Pairwise comparisons for each genotype (+ / - PhTX), Student's t-test, two tailed; n.s. p>0.05; ***p<0.001; ****p<0.0001.

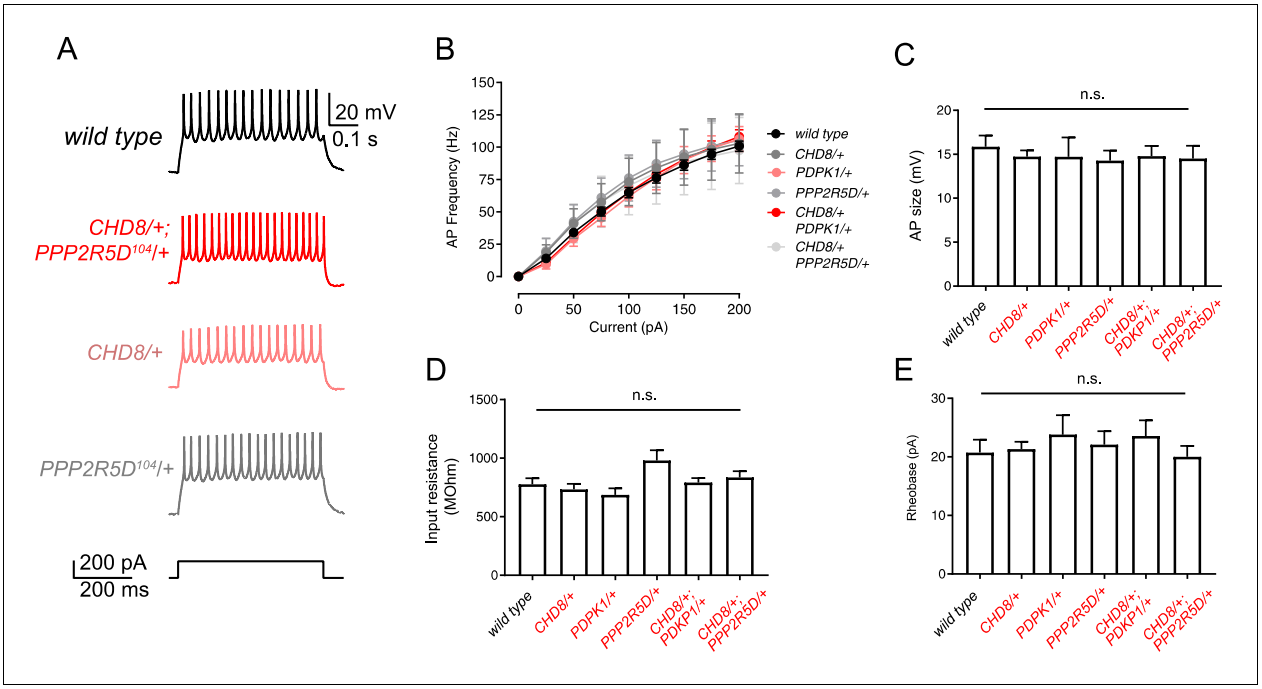

Figure 5—figure supplement 3. Firing properties of motoneurons are not different in a double heterozygous mutant. (**A**) Representative traces for motoneuron firing upon injection of 200 pA step current across indicated genotypes. (**B**), Action potential frequency is plotted against current injection amplitude for wild type and mutant as indicated. Sample sizes as follows: ***wild type*** n = 14 cells; ***CHD8/+*** n = 12 cells; ***PDPK1/+*** n = 11 cells; ***PPP2R5D/+*** n = 17 cells; ***CHD8/+; PDPK1/+*** n = 19 cells; ***CHD8/+; PPP2R5D/+*** n = 17 cells. In all instances, data were acquired from multiple animals. (**C–E**) Quantitation of action potential amplitudes, input resistance and rheobase for wild type and indicated genotypes. Sample sizes as in (**B**). One-way ANOVA and Tukey's multiple comparisons (n.s. statistically not different, p>0.05).

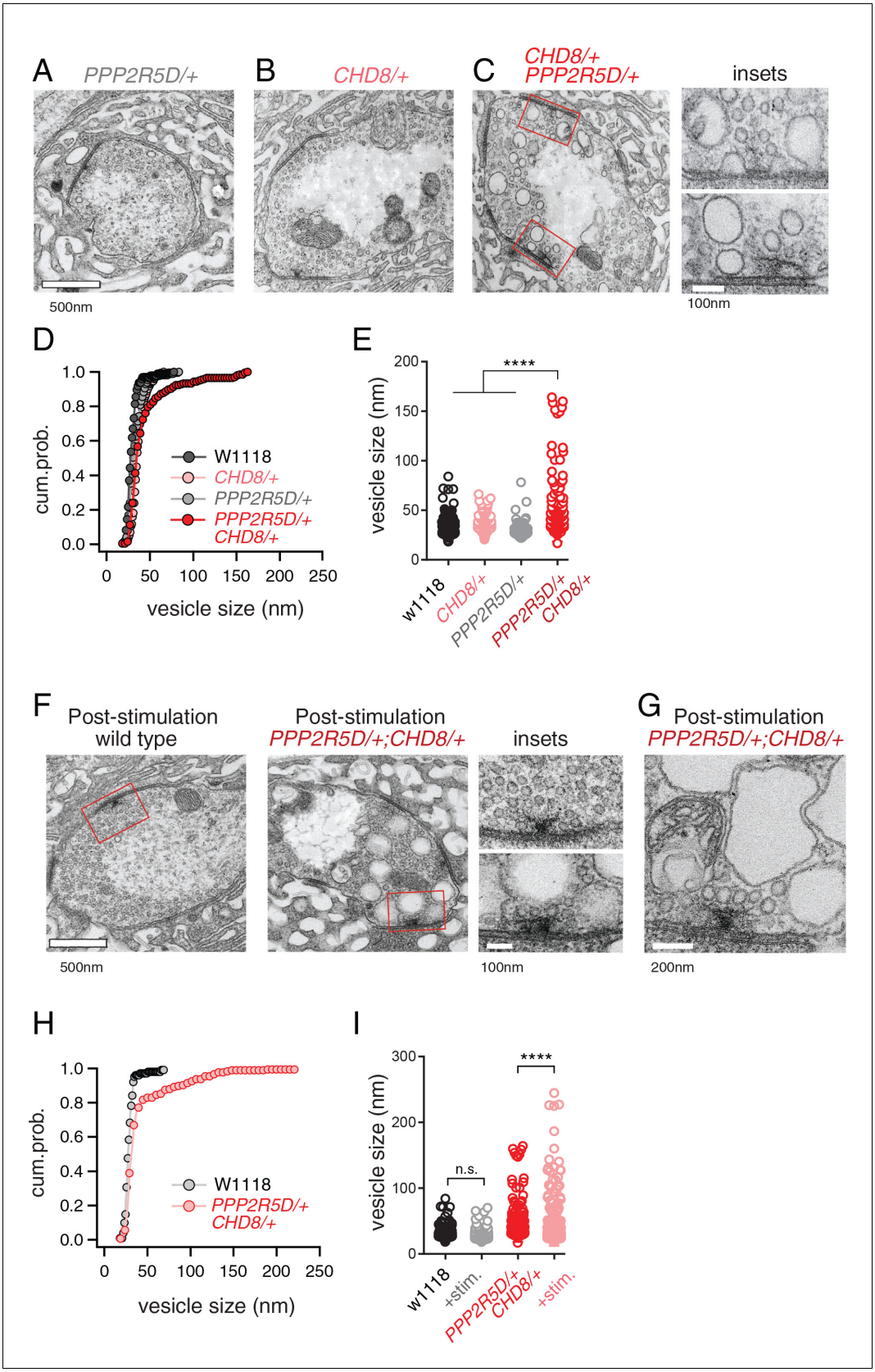

Figure 6. ASD gene-modifier interaction causes impaired synaptic membrane organization. (**A–C**) Representative electron microscopy images of individual boutons inclusive of (**A**) *PPP2R5D/+*, (**B**) *CHD8/+* and (**C**) *CHD8/+; PPP2R5D/+* double heterozygous mutant. Insets (**C**) show individual active

Figure 6 continued on next page

Figure 6 continued

zones taken from the image on the left (red rectangles) (**D**) Cumulative probability distribution of the vesicle size for wild type (*w1118*) and *CHD8/+* and *PPP2R5D/+* single mutants, as well as the *CHD8/+; PPP2R5D/+* double heterozygous mutants. Each point reflects the average at a single active zone. (**E**) Plot of individual data points for each genotype as shown in (**D**). Sample sizes (**D, E**): Animal number: w1118 N = 2, *CHD8/+* N = 2; *PPP2R5D/+* N = 2; *CHD8/+; PPP2R5D/+* N = 3. Active zone number: in same genotypic order n = 12, n = 23, n = 10, n = 14; Vesicle number n = 97, n = 171, n = 85; n = 89. (**F**) Representative electron microscopy images for individual boutons for indicated genotypes after stimulation with 50 Hz for 10 s and rapid fixation. Insets show active zones for *wild type* (top) and the *CHD8/+; PPP2R5D/+* double heterozygous mutant (bottom) taken from the images on the left (red rectangles) (**G**) An example image from the *CHD8/+; PPP2R5D+* double heterozygous mutant with larger vesicles having a crenulated appearance after stimulation. (**H**) Cumulative probability distribution of the vesicle size for wild type (*w1118*) and the double heterozygous mutant *CHD8/+; PPP2R5D/+* after stimulation and rapid fixation. Each point reflects the average at a single active zone. (**I**) Plot of individual data points for data in (**H**). Sample sizes (**H, I**): Animal number: *w1118* with stimulation N = 2, *CHD8/+; PPP2R5D/+* with stimulation N = 2; Active zone number n = 10, 21. Vesicle number n = 101, n = 175. One-way ANOVA Tukey's multiple comparisons, ****p<0.001, n.s. p>0.05.

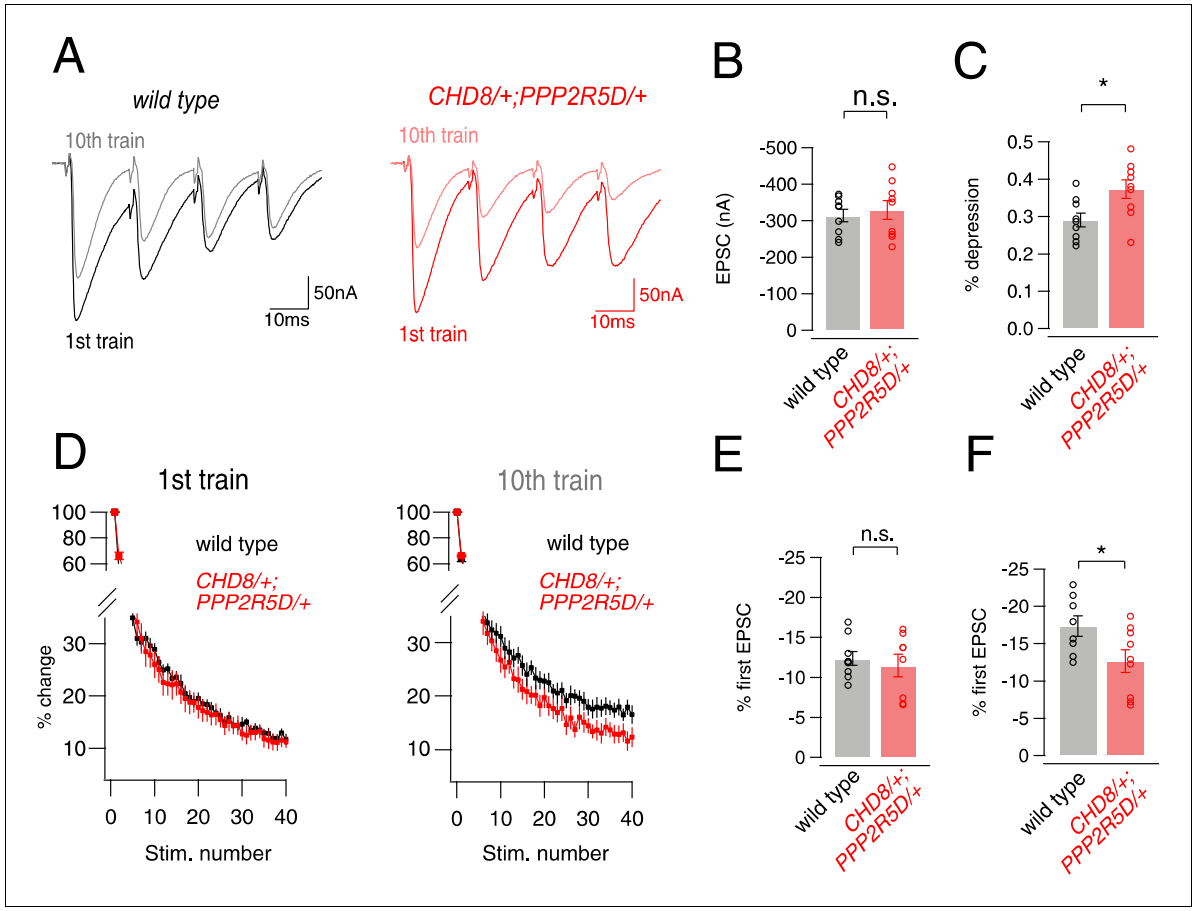

Figure 6—figure supplement 1. Analysis of short-term depression in *CHD8/+; PPP2R5D/+* double heterozygote. (**A**) Representative traces for EPSCs following 50 Hz stimulation (40 stimuli, 1st four shown for purposes of display) from *wild type* and the *CHD8/+;PPP2R5D/+* double heterozygous mutant. The first four EPSCs of the 1st and 10th trains are overlaid. (**B**), Quantitation of first EPSC amplitudes. (**C**) Percent depression of first EPSC comparing the 1st and 10th trains. (**D**) Percent change (compared to first EPSC) for EPSC amplitudes during the train are plotted for wild type and double heterozygous mutant animal, as indicated. (**E**) Quantification of the percent change in EPSC shown in (**D**) for the first train. (**F**) Percent depression of first EPSC after 10 trains. Student's t-test, two tailed; n.s. $p>0.05$; *$p<0.05$.

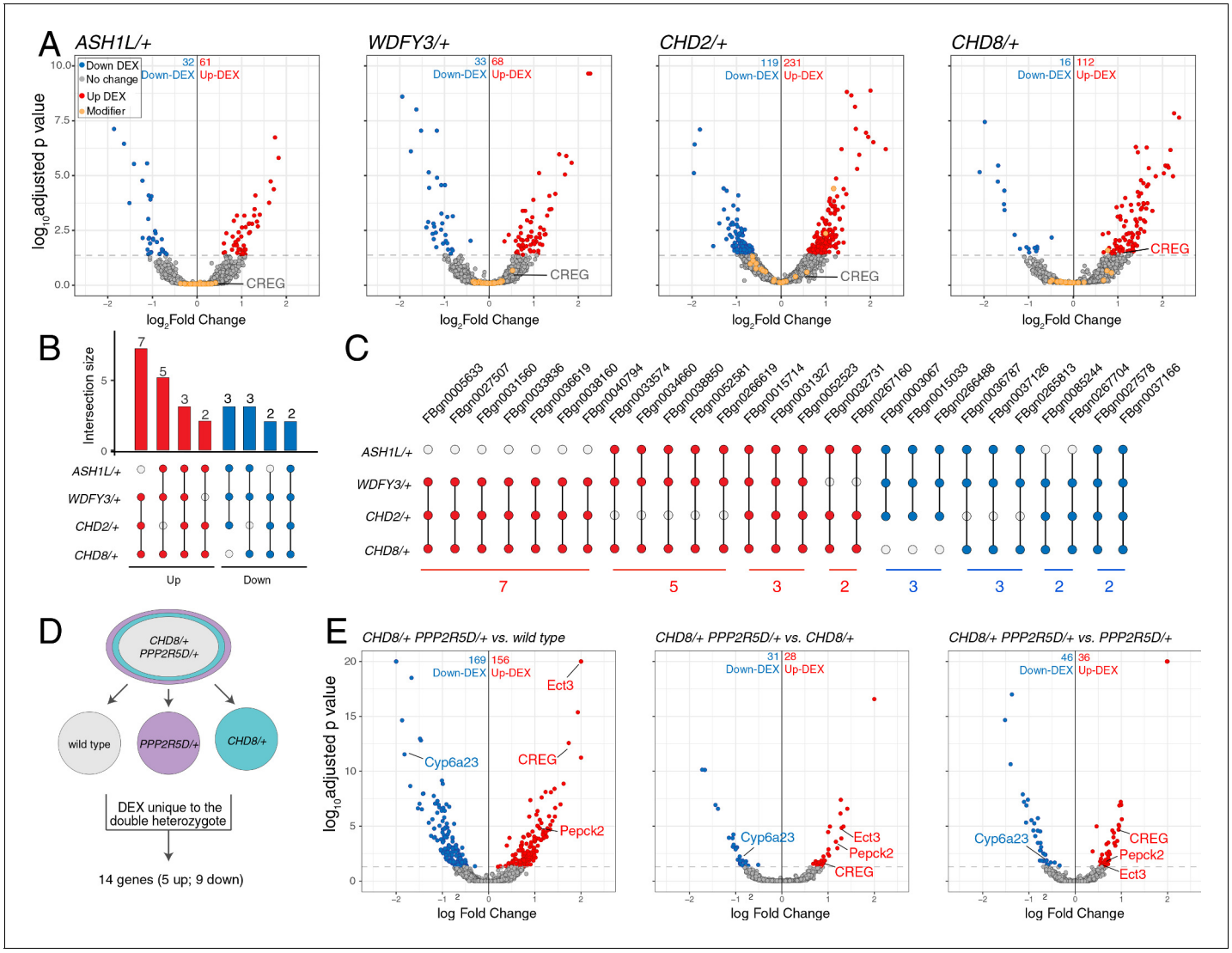

Figure 7. Differential gene expression analysis identifies *CREG*. (**A**) Volcano plot display of differentially expressed genes (DEX) for each heterozygous mutant versus wild type. Candidate ASD-gene modifiers are indicated (orange dots). Horizontal dashed line indicates cutoff of adjusted p-values (0.05). (**B**) Matrix shows all intersections of DEXs from the four indicated genotypes (see Database S1). Filled circles in the matrix indicate sets that are part of the intersection between genotypes. Bar graphs on the top show the total number of DEXs for each set, ordered by the size of intersection. (blue, up-regulated; red, down-regulated). (**C**) Individual genes are listed at the intersection of each genotypes. (**D**) Schematic showing the selection of 14 genes uniquely dysregulated in *CHD8/+; PPP2R5D/+* double heterozygous mutants. (**E**) Volcano plot display of DEX calculated as *CHD8/+; PPP2R5D/+* versus wild-type, *CHD8/+; PPP2R5D/+* versus *CHD8/+* and *CHD8/+; PPP2R5D/+* double heterozygotes versus *PPP2R5D/+* alone.

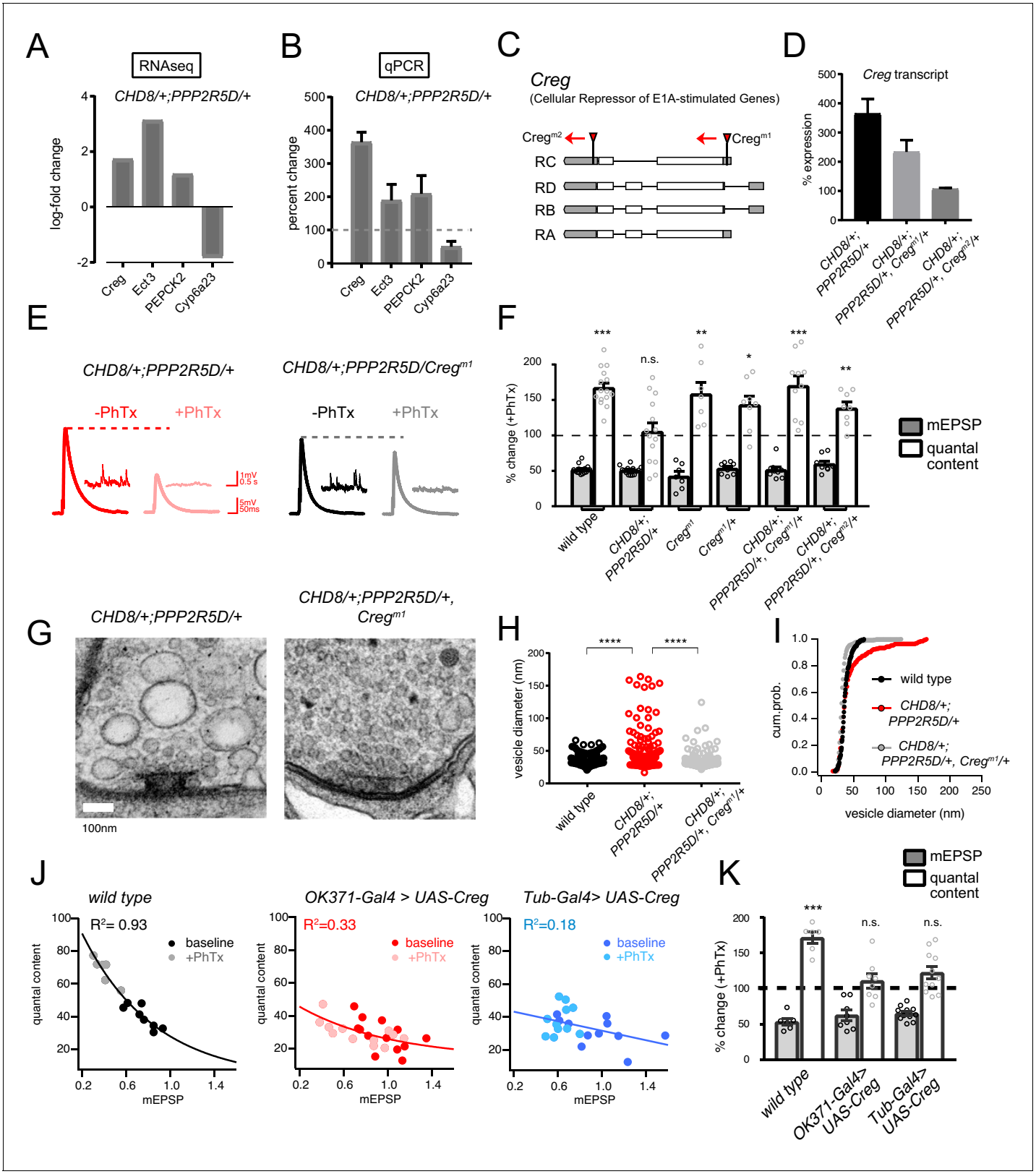

Figure 8. *CREG* is a homeostatic repressor that blocks PHP and regulates synapse ultrastructure. (**A**) Quantification of transcriptional changes calculated by RNAseq for four genes (*CREG*, *Ect3*, *PEPCK2* and *Cyp6a23*) in *CHD8/+; PPP2R5D/+* double heterozygous mutant versus wild-type. (**B**) Quantification of the transcriptional changes for the same genes in (**B**) by qPCR. (**C**) Schematic of the *Drosophila CREG* locus. The positions of two

Figure 8 continued on next page

Figure 8 continued

transposon insertion mutations are shown (red triangles). (**D**) Average *CREG* transcript levels calculated by qPCR are shown for the indicated genotypes **E**) Representative EPSP and mEPSP traces for indicated genotypes. (**F**), Bar graph (right) shows percent change in mEPSP (black filled) and quantal content (no fill) (+ / - PhTx). Sample size indicated as (–PhTx/+PhTx): ***wild type*** n = 17/15; *CHD8/+; PPP2R5D/+* n = 11/14; $Creg^{M1}$ n = 8/7; $Creg^{M1}$/+ n = 8/8; *CHD8/+; PPP2R5D/+*; $Creg^{M1}$/+ n = 8/10; *CHD8/+; PPP2R5D/+*; $Creg^{M2}$/+ n = 8/8. (**G**) Representative electron microscopy images of individual active zones from indicated genotypes (double heterozygous mutant at left, triple heterozygous mutant at right). Scale bar:100 nm. (**H**) Individual data points (vesicle size) shown for indicated genotypes. (**I**) Cumulative probability distribution of vesicle size for genotypes shown in (**H**). Sample sizes for (**H, I**): Animal number: *wild type* N = 2, *CHD8/+; PPP2R5D/+* N = 3; *CHD8/+; PPP2R5D/+;* $Creg^{M1}$/+ N = 3. Active zone number: in same genotypic order n = 12, n = 14, n = 12; Vesicle number n = 97, n = 89, n = 112. (**J**) Scatter plots of quantal content (*y* axis) versus mEPSP amplitude (*x* axis) for *wild type* (left), *OK371-Gal4 > UAS* Creg (middle, red) and *Tub-Gal4 >UAS* Creg (right, blue). Fits as indicated. R^2 values as indicated (calculated based on linear fit). (**K**) Percent change in mEPSP (gray bars) and quantal content (red bars) in presence of PhTx compared to baseline. Sample sizes as in (**F**), *wild type* n = 8/6; *OK371-Gal4 >* UAS) Creg n = 14/12; *Tub-Gal4 >*UAS) Creg n = 11/11. n.s. p>0.05, **p<0.01, ***p<0.001, ****p<0.0001.

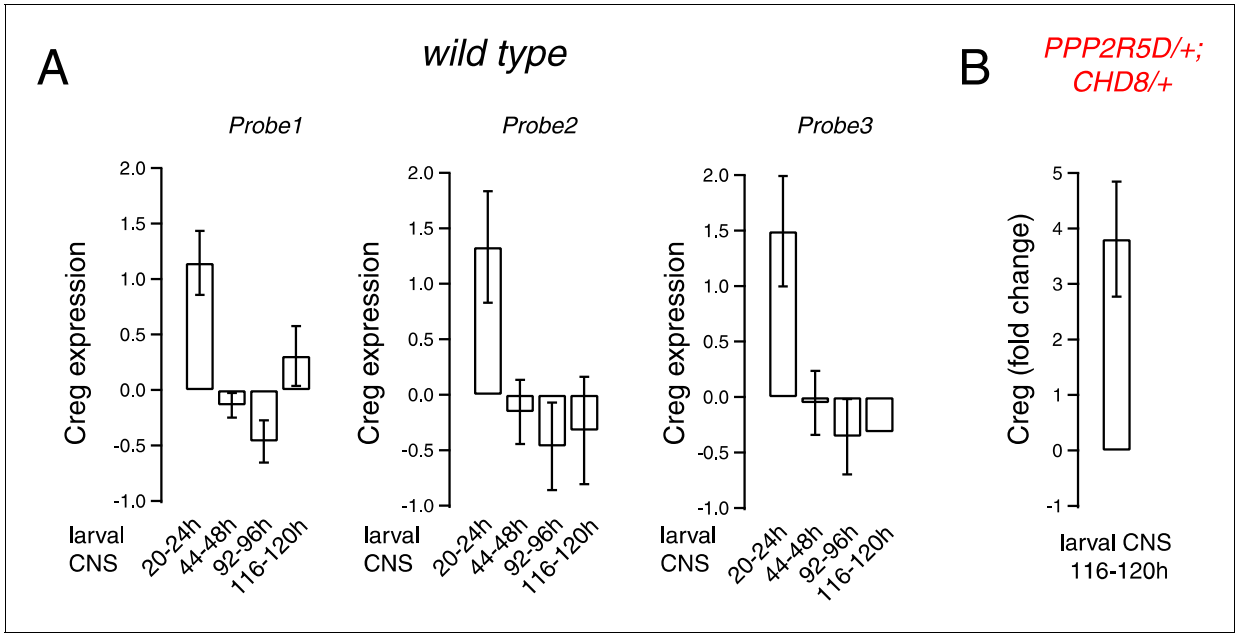

Figure 8—figure supplement 1. Expression levels of *CREG* during *Drosophila* larval development. (**A**) CREG expression levels measured in larval CNS by microarray (log2) across different developmental time points with three different probes (see from which data are derived). (**B**) Quantification of CREG expression levels for the *CHD8/+; PPP2R5D/+* double mutant compared to *wild type* by qPCR (tissue source is larval CNS).

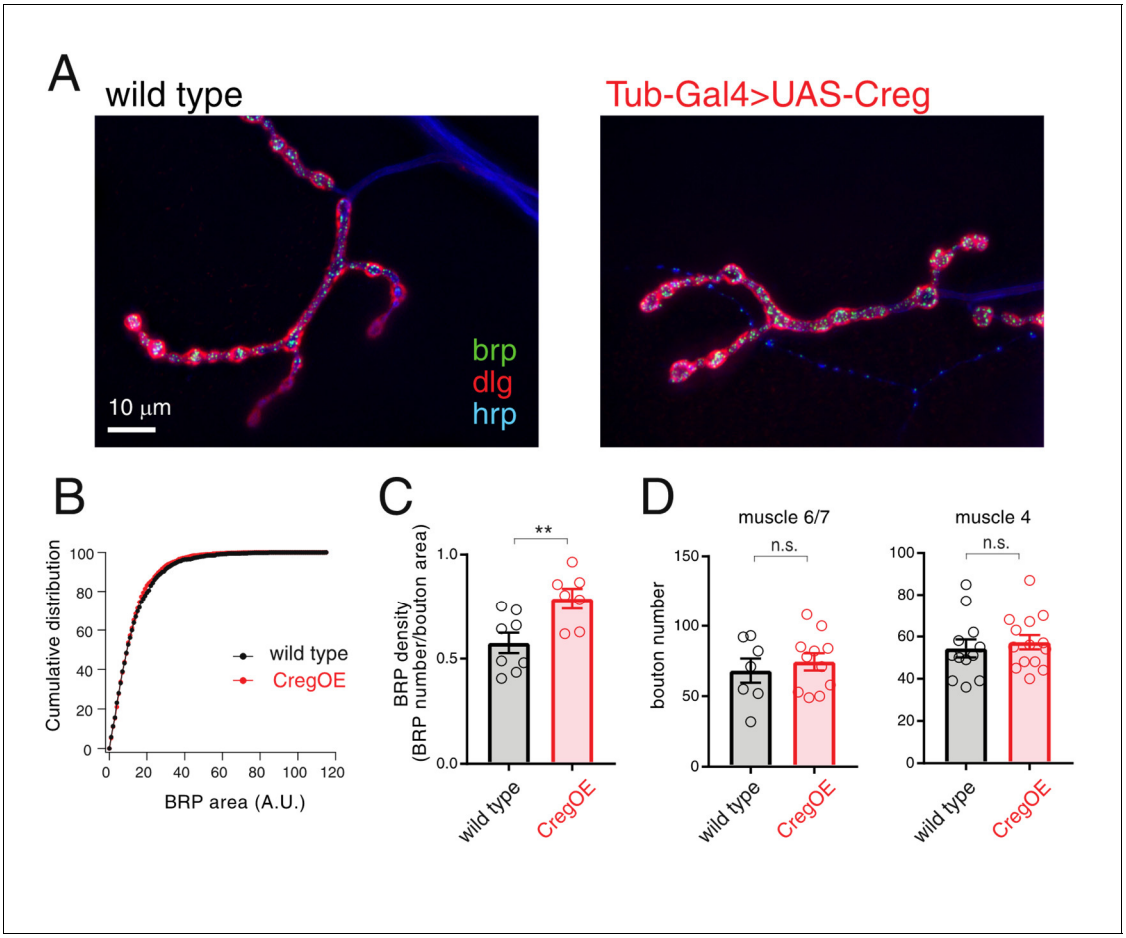

Figure 8—figure supplement 2. CREG overexpression does not substantively alter NMJ anatomy. (**A**) Immunostaining of *wild type* (left) and *Tub-Gal4 >UAS* Creg (right; CregOE) larval NMJ for Brp, DLG and HRP as indicated. (**B**) Cumulative distribution plot of BRP area for *wild type* (black) and *CregOE*. (**C**) Quantification of BRP density calculated by dividing the number of BRP positive puncta to the number of boutons. (**D**) Quantification of bouton numbers in muscle 6/7 (left) and muscle 4 (right) for the wild type (black) and *CregOE* (red). Student's t-test, two tailed; n.s. p>0.05; **p<0.01.

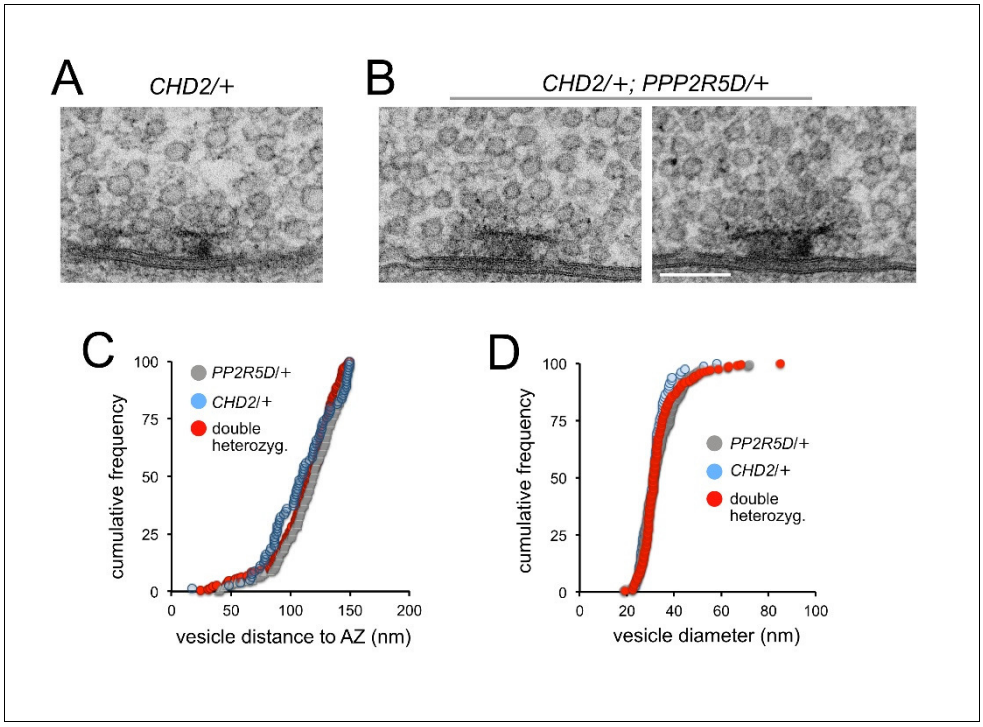

Figure 8—figure supplement 3. Ultrastructure analysis of the *CHD2/+; PPP2R5D/+* double heterozygous mutant. (**A**) Representative example of the *CHD2/+* single heterozygous mutant NMJ. (**B**), Two representative examples of the double heterozygous mutant. The membranes of the synaptic cleft are clearly defined as are clusters of synaptic vesicles of typical morphology and the electron dense T-bar structures. (**C**) Quantification of vesicle distance to the active zone for all vesicles within 150 nm radius of the T-bar centroid. (**D**) Quantification of the distribution of synaptic vesicle sizes for the indicated genotypes. Sample sizes: ***PPP2R5D/+*** = 2 animals, 31 active zones and 228 vesicles; ***CHD2/+*** = 2 animals, seven active zones and 81 vesicles; ***PPP2R5D/+; CHD2/+*** = 3 animals, 22 active zones and 204 vesicles.

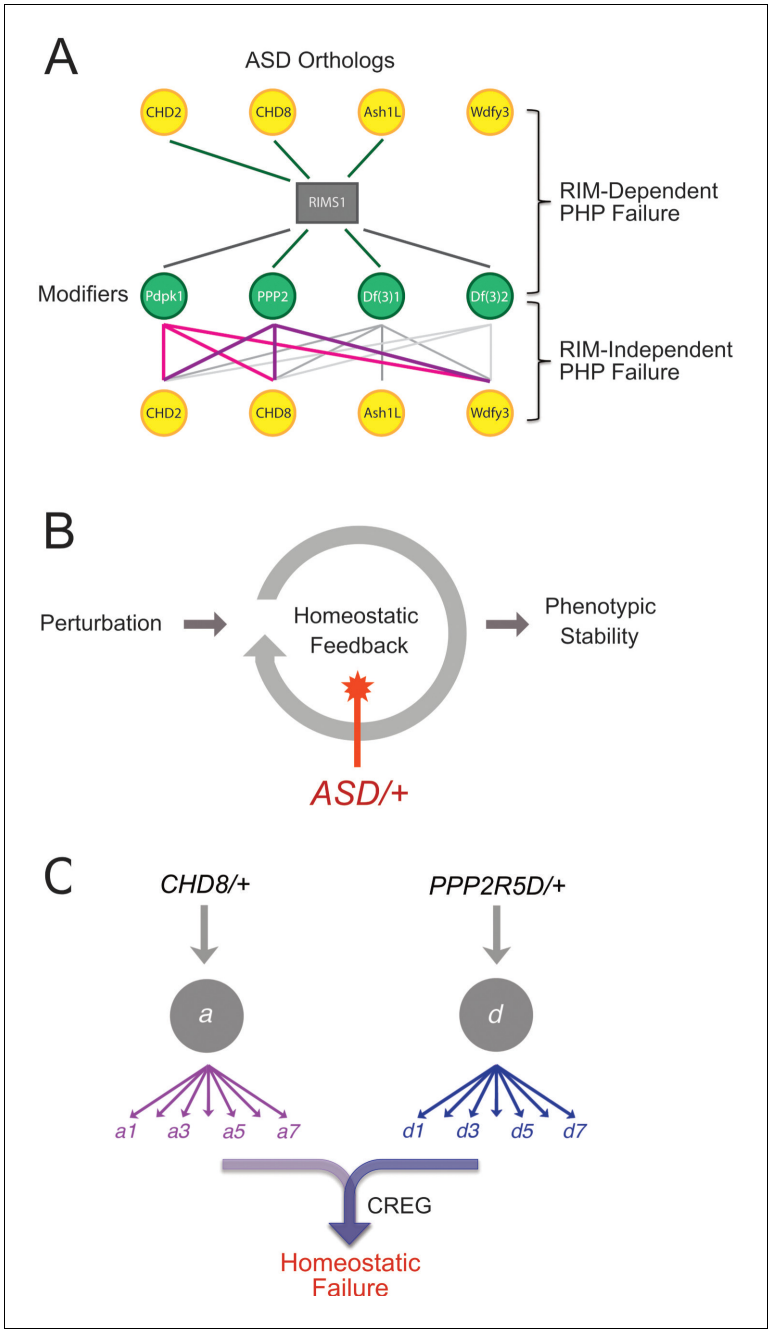

Figure 9. Summary and Model. (**A**) Summary of genetic interactions. *RIMS1* interacts with three of four ASD gene orthologues, impairing PHP. *RIMS1* interactions identified in a genetic screen as modifiers are shown below in green. Each modifier interacts with multiple ASD heterozygous mutations in a *RIMS1* independent manner, disrupting PHP. The data present a complex network of gene-gene interactions (yellow and green) that diminish the robustness of PHP. Df(3)1 refers to *Df(3)7562* and Df(3)2 refers to *Df(2)24953*. (**B**) Homeostatic signaling systems robustly ensure stable neural function. However, the homeostatic signaling system itself is sensitive to genetic perturbation. We demonstrate that PHP is sensitive to mutations in multiple genes that were identified as ASD risk factors. In at least one instance, this is due to the up-regulation of a PHP interfering factor (*CREG*) and the red star indicates this a possible mechanisms more generally. (**C**) Complexity of interpreting double heterozygous gene-gene interactions. Signaling systems are not blocked by heterozygous gene mutations, but are likely to be attenuated to some degree. The combined effect of two higher-order heterozygous gene mutations creates a downstream, intersectional effect that is very difficult to predict. In the case of this paper, we succeeded in identifying a novel intersection causing up-regulation of *CREG*, which disrupts the homeostatic signaling system.